Acrylic pressure-sensitive adhesives with nanodiamonds and acid-base dependence of the pressure-sensitive adhesive properties

Mizutani, Kota
Hongo, Chizuru
Matsumoto, Takuya
Nishino, Takashi

(Citation)
Journal of Applied Polymer Science,135(23):46349-46349

(Issue Date)
2018-06-15

(Resource Type)
journal article

(Version)
Accepted Manuscript

Acrylic Pressure Sensitive Adhesive with Nanodiamond and Acid-Base Dependence of Pressure Sensitive Adhesive Properties

Kota Mizutani[a], *Chizuru Hongo*[a], *Takuya Matsumoto*[a], *Takashi Nishino**[a]

[a]Department of Chemical Science and Engineering, Graduate School of Engineering, Kobe University, Rokko, Nada, Kobe, 657-8501, Japan

Key Word

Nanodiamond, Acrylic Pressure Sensitive Adhesive, Soap-free Emulsion Polymerization, Tack, Peeling, Holding

ABSTRACT

High performance and functional properties of pressure-sensitive adhesives (PSAs) are attractive in fundamental and industrial fields. In order to control the performance of PSAs, nanofillers were loaded in PSAs. In this study, we focused on the composites of acrylic PSAs and nanodiamond. The loaded nanodiamond reinforced their mechanical properties and increased the PSA performance. Nanodiamond in a PSA formed a network structure. It is revealed that the acidic-basic state was a key factor for the control of the dispersion of nanodiamond. When the PSA emulsions and nanodiamond aqueous dispersion was mixed under basic condition, the composites demonstrated higher PSA properties (tack, holding and peeling strength). We investigated the effect of nanodiamond loading on the PSA properties from the viewpoints of nanostructure and acid-base interaction.

Introduction

In the field of electronic devices, pharmacy, package, labels and cosmetics, pressure-sensitive adhesives (PSAs) have attracted much attentions from the viewpoints of utility, cost and recycle[1]. PSAs adhere solid substrates such as metals or resins with little contact pressure and a short contact time. In PSAs as adhesive products, various parameters of adhesive properties are required. In particular, the three major properties, tack, holding time and peeling force, are focused on for the evaluation of PSAs[2,3]. For the access to the desired properties, the control of molecular weight and crosslinking density as well as various modifications of base polymers and the loading of additives such as tackifiers and inorganic fillers have been investigated[4]. It is often the case that the phase separation and agglomeration of additives lead to the mechanical and functional defects[5]. Thus, in the cases of loading additives, the dispersion is a key factor for the high performance of PSA. In addition to the improvements intrinsic performance, other functional properties are required in the industrial products; for example transmittance, insulation resistance, electronic conductivity and thermal conductivity[6]. Their functional properties are indispensable in the electronic devices and displays. Moreover, PSAs obtained from water in oil emulsion are attractive non-VOC materials from the viewpoint of the environmental conservation[7].

Numerous inorganic nanofillers have been attempted to incorporate in PSAs, then the reinforcement and the functionalization of their nanocomposites have been reported for several decades[8–11]. Carbon nanofillers such as carbon nanotubes[8–10] and graphene[12–14] possess excellent mechanical, electrochemical and thermal properties. Nanodiamond (ND) has been produced by the detonation method, and appears as a nano-sized diamond with a diamond core and graphite-like shell[15–18]. Therefore, ND shows superior mechanical properties and thermal conductivity originated from diamond, which possesses the highest modulus and thermal conductivities in

natural minerals. In addition, its high wear resistance, hardness and biocompatibility have also been well-known[19]. The surface of ND contains various hydrophilic functional groups such as carboxyl, hydroxyl and ether groups, and so ND is obtained as aqueous dispersion[20–22]. In the case of nanocomposites with hydrophobic polymers, the preparation methods and dispersion of ND fillers in polymer matrixes control their performances.

Herein, we focused on the PSA properties and morphology of the polyacrylates/ND nanocomposites and the interaction between ND and polyacrylates. We employed two types of polyacrylates; one was poly(*n*-butyl acrylate-acrylic acid) (P(BA-AA)) and the other was poly(*n*-butyl acrylate-glycidyl methacrylate) (P(BA-GMA)). Both polymers were widely accepted as conventional PSA matrixes.[23–26] The nanocomposites were prepared by mixing polyacrylate-type emulsion and ND aqueous dispersion. This preparation in aqueous media led to a well-dispersion in the PSA composites. We assessed the effect of acidity of PSA and dispersion of ND into PSA on PSA and mechanical properties. The reinforced effect of ND on PSA properties and the formation of ND network in PSA composites were evaluated from the mechanical property, morphology and chemical structure. Moreover, we investigated the effect of the pH of PSA/ND emulsion on the PSA properties.

Experimental Section

Materials

n-butyl acrylate, acrylic acid and glycidyl methacrylate (BA, AA and GMA, Nacalai tesque, Inc.), as monomers and potassium peroxodisulfate (KPS, Sigma Aldrich), as initiator, were used without any purification.

ND aqueous suspension (2.75 %w/w) was supplied from Bando Chem. Ind. ND powder was produced by the detonation of explosives such as TNT (2-methyl-1,3,5-trinitrobenzene) and RDX (hexahydro-1,3,5-trinitro-1,3,5-triazine) under an inert atmosphere. The detonation soot was purified using liquid oxidants, followed by annealing and rinsing. After removing the impurities, ND powder was nanodispersed in water and individualized by wet milling process with bead mill.

Sample preparation

We performed soap-free emulsion polymerization for the preparation of P(BA-AA) and P(BA-GMA) emulsions. Deionized water (450 g), BA monomer (45 g), AA or GMA monomer (5 g) and KPS (0.5 %w/w vs. monomer) were sequentially added to the flask. The mixture was then stirred at 200 rpm at 70 °C for 8 h. The emulsions were stabilized by the electric hindrance through the sulfate groups on the particle surface against coagulation[27]. The yields were calculated from weights of solid residuals after drying emulsion.

The PSA/ND nanocomposites were prepared by a simple casting method. First, ND aqueous suspension was ultrasonicated for 1 h. Then it was added to the emulsion and stirred for 1 day. After that, the PSA/ND aqueous suspension was cast and dried at 40 °C. The amounts of added ND were 0, 1, 5 and 10 wt% vs PSAs.

Characterization

Raman spectra of the emulsion were recorded on a confocal nanoRaman microscope (ALPHA300R, WITec). The wavelength of the Nd/YAG laser was 532 nm.

The average molecular weight of the synthesized PSAs was analyzed by gel permeation chromatography (HITACHI L-7000 Series, Shimadzu Co.) as 0.5 wt% solutions in tetrahydrofuran and it was detected with refractive index spectrometer (HITACHI L-7490, Shimadzu Co.). The TSK gel GMHHR-M column (Tosoh Corp.) was used with a flow rate of 1 mL/min at 40 °C. The molecular weight was calibrated with polystyrene standard.

The diameter of the PSA particles were observed with fiber-optics particle analyzer (FPAR-1000RK, Otsuka electronics).

X-ray diffractometer (RINT2100, Rigaku) was operated at 40 kV/20 mA using Ni-filtered CuKα radiation. The $2\theta/\theta$ scan data were collected at 0.02 degree intervals with a scanning speed of 1.0 degree/min.

Thermogravimeter (TG) (Thermo plus EVO2 TG8121, Rigaku) was used at a heating rate of 10 °C/min under nitrogen flow. The temperature of 5 % thermal weight loss was defined as the thermal decomposition temperature (T_{d5}).

The tack properties of the prepared PSA composites were measured through J. Dow-type rolling ball tack tests in room temperature as shown in Figure S2 in Supporting Information. The tack was evaluated using the ball number, which was expressed by multiplied the ball diameter (inches) 32 times. The maximum ball number where the ball stopped on the PSA with 30° slope for longer than 5 min is defined as the tack.

Holding time was measured using thermomechanical analyzer (TMA, Thermo plus EVO TMA8310, Rigaku). A heating rate was 3 °C/min under nitrogen flow. The instrument was operated in tension mode under 8.3 MPa stress.

For 180° peel tests, PSAs were casted on PET films with 40 μm thickness. Each sample was then attached to a glass plate by loading 0.40 kg weight 10 times. 180° peel tests were performed using universal testing machine (Autograph AG-X plus (Shimadzu Co.)). The peeled specimens were 10 mm width and 30 mm length. The angle between the tensile direction and glass plates was 180° and the peeling speed was 300 mm/min.

The tensile tests were performed using Autograph AG-X plus (Shimadzu Co.). The specimens were uniaxially tensiled with a cross head speed of 300 mm/min. The initial length, width and thickness were 10 mm, 5 mm and 200 μm, respectively. The toughness (K) was calculated as follows:

$$K = \int_{\varepsilon=0}^{\varepsilon=\varepsilon_{\max}} \sigma \cdot \mathrm{d}\varepsilon / \rho \quad \text{(J/g)} \qquad (1)$$

where σ is the stress (Pa), ε is the strain, and ρ is the density (g/m^3). These experiments were performed for at least 5 different specimens, then the averaged values and their standard deviations were calculated.

Dynamic mechanical analyses (DMA) were carried out with tensile mode using a dynamic mechanical analyzer (DVA-220S, ITK Co., Ltd.) under nitrogen flow. A heating rate was 3 °C/min, and a frequency of 2 Hz were employed.

Thermal conductivity (λ) was obtained by measuring thermal diffusivity (α) (Thermowave analyzer TA3, BETHEL)[28]. α value measured at five different points for each sample, and the averages were regarded as the experimental value α. Thermal conductivity λ was calculated from the following equation.

$$\lambda = \rho \cdot \alpha \cdot C_p \qquad (2)$$

where C_p is specific heat. C_p were measured using a different scanning calorimeter (DSC) (Thermo plus EVO DSC8230, Rigaku) at the heating rate of 5 °C/min.

Atomic force microscopic (AFM) observation was performed on the PSA/ND composites with a NanoNavi□/E-sweep (Hitachi high-tech science coorporation). A silicon cantilever probe (SI-DF20) was used in the dynamic force mode (DFM) in air.

Microstructures of the samples were observed with transmission electron microscope (TEM) (JEM-2100F, JEOL) at an accelerating voltage of 200 kV. In the TEM observation, the Cu grid with elastic carbon supporting films and the non-supported grid were employed for composites and ND, respectively.

Results and Discussion

Characterization

We synthesized the polyacrylate PSAs through a soap-free emulsion polymerization of BA and AA, or BA and GMA combinations. The weight ratio of BA and AA or GMA in the soap-free emulsion polymerization was 90% and 10%, respectively. From Raman spectra of the synthesized PSAs, it is revealed that the polymerization progressed and the BA ratios were sustained even after polymerization, as shown in Figure S3 in Supporting Information. The Raman bands originated from the C=C double bonds of BA, AA and GMA monomers were observed at around 1650 cm^{-1} [29]. After polymerization, these bands disappeared. The weight-average molecular weight of the synthesized PSAs were 165,000. P(BA-GMA) was insoluble to common organic solvents such as tetrahydrofuran. It is suggested that crosslinking of epoxy groups should occur under polymerization. However, most epoxy groups were sustained because Raman scattering bands of epoxy groups of P(BA-GMA) were observed at 1275 cm^{-1} clearly.[23,30] The yields were 97% and 98%. The effective polymerization was achieved and their molecular weights were sufficient for applying to PSAs. The polymerized emulsions were obtained as 10 wt% aqueous dispersion. The particle sizes in PSA emulsion were measured by dynamic light scattering (DLS), as shown in Table S2 in Supporting Information. The size of P(BA-AA) and P(BA-GMA) particles were 548 nm and 465 nm, respectively. Their sizes were ten times larger than that of ND in aqueous dispersion.

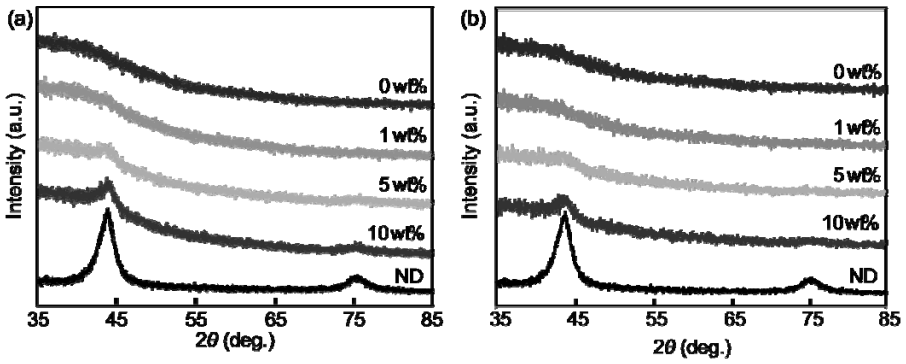

Figure 1. X-ray diffraction profiles of (a) P(BA-AA)/ND and (b) P(BA-GMA)/ND with various ND contents.

The composites were prepared by adding the 2.75 wt% ND aqueous dispersion into the synthesized PSA emulsions. After mixing ND and PSAs, the aqueous dispersion were cast and dried for 3 h at 40 °C. The amounts of ND in the PSA/ND composites were 0, 1, 5 and 10 wt% vs PSAs. The thickness of the PSA sheets were around 40 μm. In order to characterize the loaded ND, we measured their X-ray diffraction and thermogravimetric analyses.

Figure 1 shows X-ray diffraction profiles of P(BA-AA)/ND and P(BA-GMA)/ND composites. The X-ray di□raction peaks were observed clearly for the ND particles at 2θ = 43.9° and 75.3°, respectively, which could be assigned as 111 and 220 reflections of diamond structure.[31] These indicate that the ND particles possess three-dimensional diamond structure even at a size of no more than 10 nm. In the profiles of the PSA/ND nanocomposites with ND contents over 5 wt %, the diffraction peak was detected at 2θ = 43.9° and 75.3°. These results suggested that ND was certainly loaded into the PSA composites and the crystalline structure of ND remained unchanged in the composites. The thermos-gravimetric trace charts of the prepared composites are shown in Figure 2. Their thermal decomposition temperatures at 5 wt% loss (T_{d5}) are shown in Table 1. In both PSA composites, the thermal decomposition originated from PSAs was observed at around

330 °C. T_{d5} of the P(BA-AA) composites stayed unchanged after ND was loaded, while P(BA-GMA) composites were stabilized thermally and their T_{d5} increased[32,33]. The amounts of residues of their composites were increased with loading of ND. The weight loss of ND at 500 °C was hardly observed. Therefore, the residues of composites can be speculated to be originated from the loaded ND. The amounts of the residues in both nanocomposites corresponded to those of added ND.

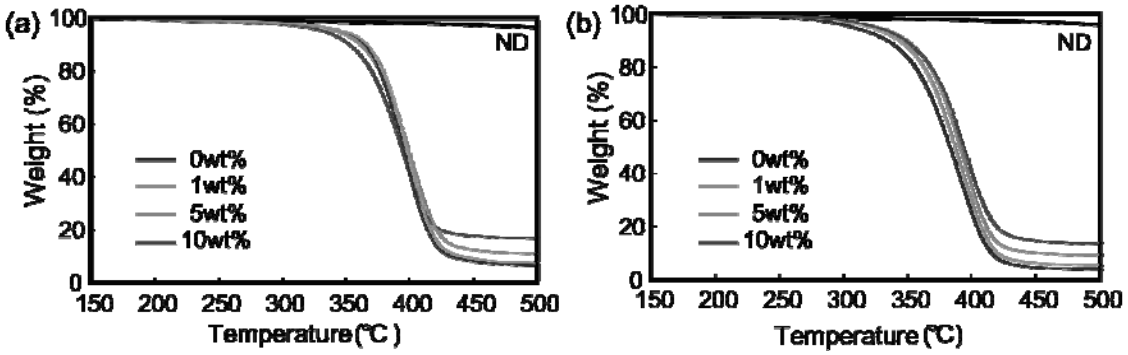

Figure 2. Thermo-gravimetric traces of (a) P(BA-AA)/ND PSA and (b) P(BA-GMA)/ND composites.

Table 1. Thermal decomposition temperature and ND content of P(BA-AA)/ND and P(BA-GMA)/ND composites.

ND contents	T_{d5} °C	ND content (obsd.) %
ND	557	–
P(BA-AA) PSA none	347	0
1 wt%	346	0.7
5 wt%	343	4.3
10 wt%	333	9.9
P(BA-GMA) PSA none	313	0
1 wt%	321	1.6
5 wt%	324	5.6
10 wt%	326	10.6

Table 2. Tack and holding time for peel resisitance at 40 °C and 70 °C for the P(BA-AA) and P(BA-GMA) with 0, 1, 5 and 10 wt% of ND.

ND contents	Tack ball number	Holding time at 40 °C (h)	Holding time at 70 °C (h)
P(BA-AA) PSA none	7	>24	0.7
1 wt%	7	>24	0.9
5 wt%	7	>24	1.1
10 wt%	5	>24	1.8
P(BA-GMA) PSA none	9	>24	0.6
1 wt%	10	>24	1.5
5 wt%	11	>24	>24
10 wt%	10	>24	>24

PSA properties.

For the evaluation of PSA properties, we focused on tack, holding time and 180 ° peel strength of P(BA-AA) and P(BA-GMA) PSA.

In the tack tests, we employed rolling ball tack tests. The ball number of P(BA-AA) kept constant with or without ND. In the P(BA-AA) composites with 10 wt% ND, the ball number decreased. On the other hand, the ball numbers of P(BA-GMA)/ND composites were larger than those of P(BA-AA)/ND. Moreover, the loading of ND enhanced the tack in P(BA-GMA) composites and the maximum tack was achieved by loading of 5 wt% ND.

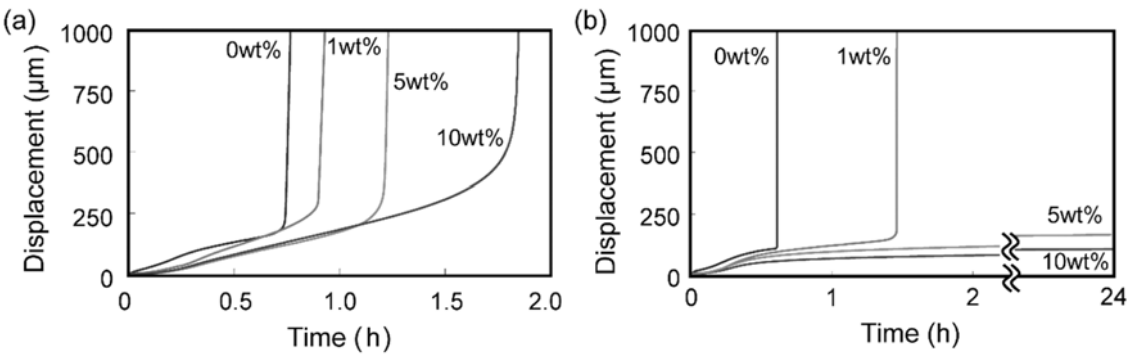

Figure 3. Holding tests under 8.3 MPa at 70 °C of (a) P(BA-AA)/ND and (b) P(BA-GMA)/ND composites with 0, 1, 5 and 10 wt% of ND.

We measured the holding time of the prepared PSA composites under 8.3 MPa loading at 70 °C. When the holding tests were carried on at 40 °C, the high holding time more than 24 h were observed for all the PSA composites. In contrast, the holding time of P(BA-AA) composites at 70 °C were increased, as shown in Figure 3. The holding time of P(BA-GMA) without ND was similar to that of P(BA-AA), while the loading of ND into P(BA-GMA) increased the holding time drastically. The holding time of P(BA-GMA) containing 5 and 10 wt% ND were more than 24 h. In the P(BA-GMA)/ND composites, the ND loading effect were prominently emerged, relative to P(BA-AA)/ND composites.

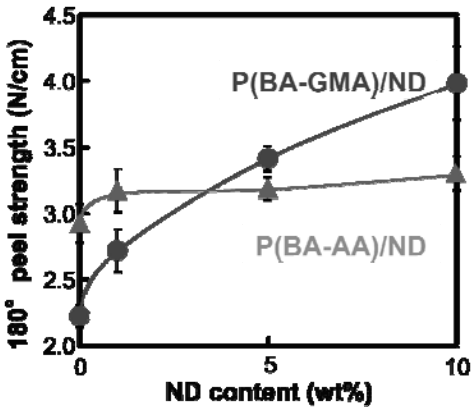

Figure 4. 180° peeling strength of P(BA-AA)/ND and P(BA-GMA)/ND composites with 0, 1, 5 and 10 wt% of ND.

In the 180° peel tests, the ND loading effects were observed in both PSA composites, as shown in Figure 4. The 180° peel strength of P(BA-AA)/ND composites were almost plateau regardless

of ND contents, whereas the strength of P(BA-GMA)/ND composites raised gradually as the amounts of ND in the composites increased. The 180° peel strength of P(BA-GMA) PSA were lower than that of P(BA-AA). However, the peel strength of P(BA-AA) and P(BA-GMA) composites with more than 5wt% ND were inverted. These results suggest that the loading of ND contributed largely to adhesive properties of P(BA-GMA) composites rather than those of P(BA-AA)-based PSA.

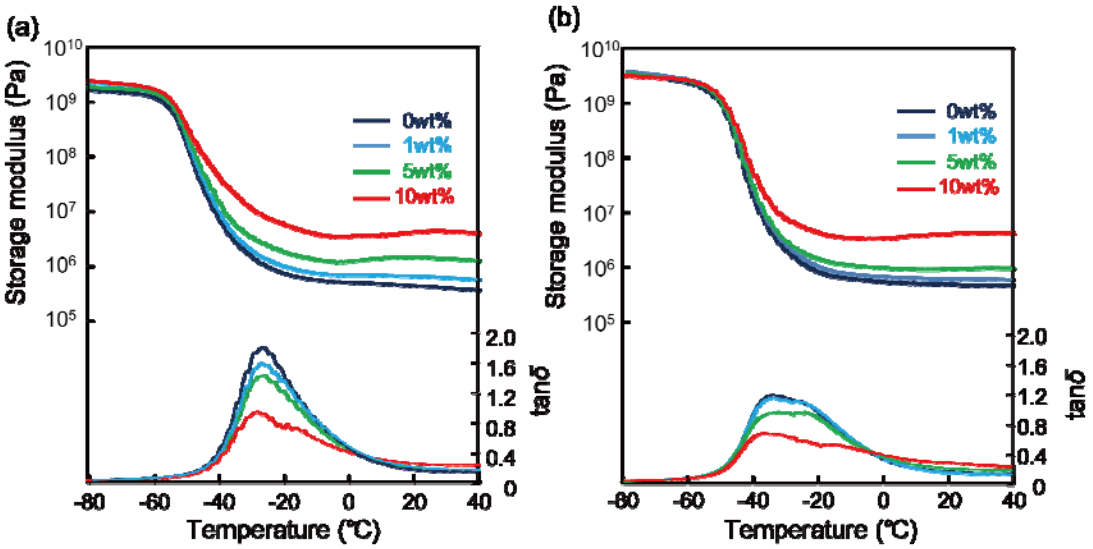

Figure 5. Storage modulus (upper) and tan δ (bottom) of (a) P(BA-AA)/ND and (b) P(BA-GMA)/ND composites with 0, 1, 5 and 10 wt% of ND.

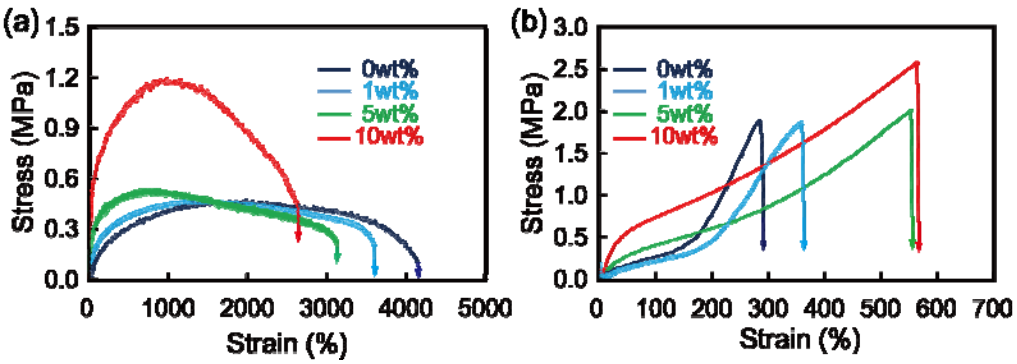

Figure 6. Stress-strain curves of (a) P(BA-AA)/ND and (b) P(BA-GMA)/ND composites with 0, 1, 5 and 10 wt% of ND.

Mechanical and thermal properties.

For further investigation of ND loading effects in PSA composites, their mechanical properties were measured with DMA and tensile tests.[5,34–36]

Figure 5 and 6 show DMA charts and stress-strain curves, respectively. Table S3 in Supporting Information summerized detail data of the mechanical properties of the PSA composites. The storage modulus of P(BA-AA)/ND and P(BA-GMA)/ND composites increased with ND contents. In addition, the glass transition temperatures of P(BA-AA) and P(BA-GMA) without ND were observed at −35 °C and −25 °C, respectively. The loading of ND led to a decrease of the peak intensity of tan δ and the increase of that in the higher temperature region. These means that the loss modulus were decreased relatively to the storage modulus. In contrast, their T_g were independent on loading of ND. In the P(BA-AA)/ND composites, their strains at break decreased with ND contents, while their Young's modulus and toughness increased. All the mechanical parameters of P(BA-GMA)/ND composites, namely Young's modulus, elongation at break and toughness, were increased by loading ND. The effective reinforcement of ND in P(BA-GMA) PSA was observed rather than in P(BA-AA). As mentioned above, these three mechanical properties controlled their PSA properties, that is, tack, holding time and peeling strength. Stringiness of PSA was one of decisive factors for these PSA properties. The increases of Young's modulus, elongation at break and toughness of P(BA-GMA)/ND composites would lead to the reinforcements of stringiness, which results in the higher PSA properties.

The high thermal conductivity of ND is well-known[31]. We measured the thermal conductivity of the PSA/ND composites in the in-plane and thickness directions as shown in Figure 7. In both directions, the conductivities of P(BA-GMA) with various ND contents were larger than those of P(BA-AA). In the thermal conductivity of both PSA composites in the thickness direction, the ND loading effects were not observed, while the thermal conductivities in the in-plane direction were increased with larger contents of ND.

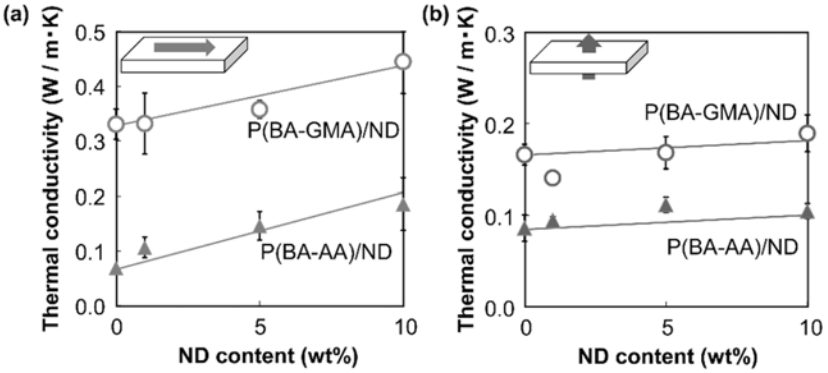

Figure 7. Thermal conductivity of P(BA-AA)/ND and P(BA-GMA)/ND composites with different ND contents to the (a) in-plane and (b) thickness direction.

Morphology

For the deeper insight on the reinforced effect of ND, we investigated the morphology of P(BA-AA)/ND and P(BA-GMA)/ND by AFM and TEM. Figure 8 showed the topological geometries and phase images of P(BA-AA) and P(BA-GMA) PSA. In the P(BA-GMA), the particles were clearly observed compared to P(BA-AA). This is because P(BA-AA) possessed higher Young's modulus and their deformation was prevented. The particle configuration were represented more clearly in phase images. The observed particle sizes were 409 nm, which corresponded to that 465 nm obtained by DLS measurements. In addition, Figure 9 shows the TEM

images of ultrathin cross section of a) P(BA-AA)/10wt%ND and b) P(BA-GMA)/10wt %ND. ND in PSA matrixes was observed without any staining. In the P(BA-AA)/10wt%ND, ND particles were dispersed randomly, while, in the P(BA-GMA)/10wt%ND, the network structure of ND and P(BA-GMA) particles were observed as shown in Fig. 9 (b). The observed particle size also corresponded to the results in DLS measurements and AFM images. The network would be expanded in the P(BA-GMA) composites three-dimensionally. Therefore, in the P(BA-GMA)/ND PSAs, the effect of ND loading on the PSA properties were prominently observed.

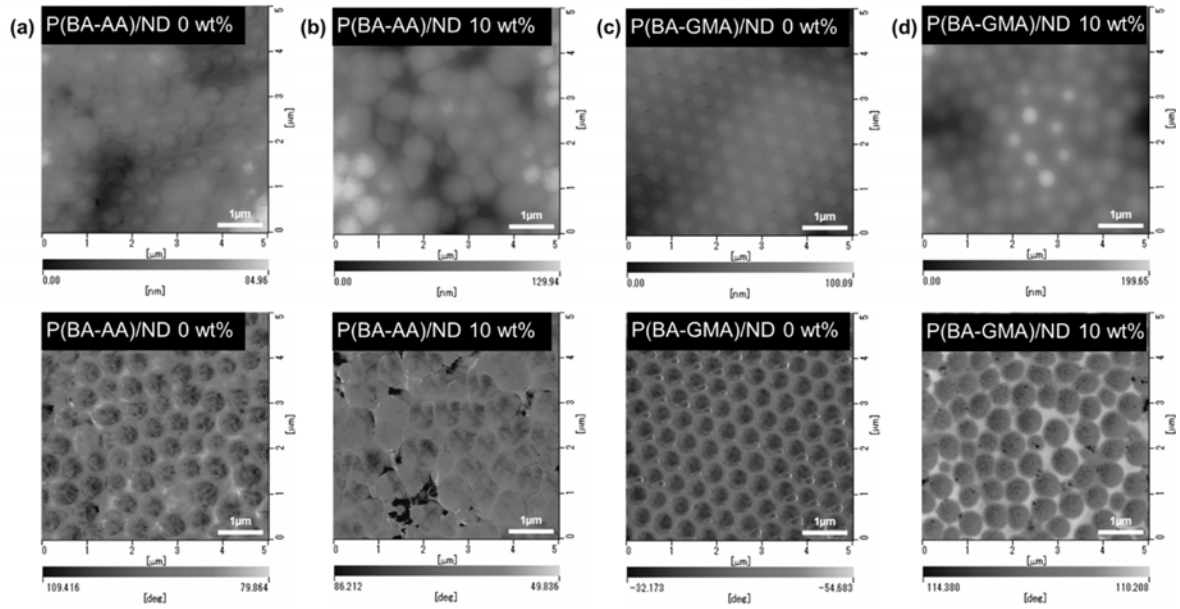

Figure 8. Topological geometries (upper) and phase images (bottom) of (a) P(BA-AA), (b) P(BA-AA)/10wt%ND, (c) P(BA-GMA) and (d) P(BA-GMA)/10wt%ND.

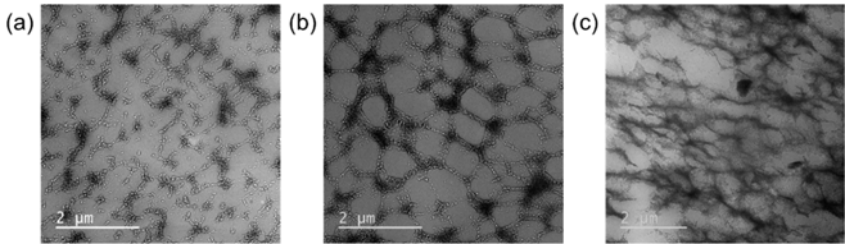

Figure 9. TEM images of (a) P(BA-AA)/10wt%ND, (b) P(BA-GMA)/10wt%ND and (c) P(BA-AA)/10wt%ND prepared at pH12.

The pH values of P(BA-AA) and P(BA-GMA) without ND were similar to each other. The pH value of ND dispersion was 11.4. In the case of P(BA-AA)/ND PSA composites, the loading of ND provided the gradual decrease of the acidity. The pH values of P(BA-GMA) containing 1wt% ND corresponded to that of P(BA-AA), while those with 5wt% and 10 wt% jumped up to more than 10. In addition, it is revealed from DLS measurements that ND in P(BA-GMA)/ND aqueous dispersion connected stiffly with P(BA-GMA) then the particle size was increased with loading ND in Table S2 in Supporting Information. These results suggested that, in P(BA-GMA)/ND aqueous dispersion, the P(BA-GMA) particles interacted strongly with ND and their surface were coated with ND.

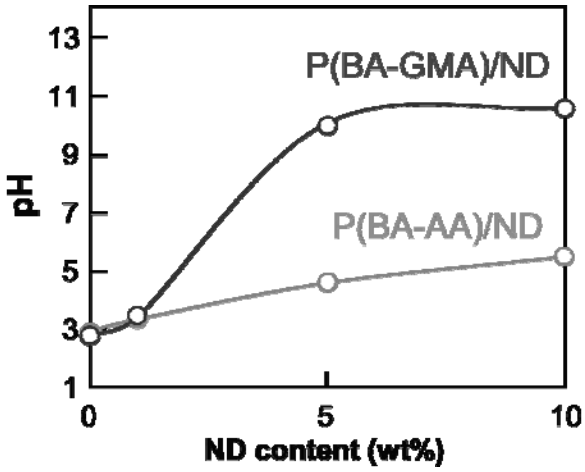

Figure 10. pH values of P(BA-AA)/ND and P(BA-GMA)/ND aqueous dispersion with 0, 1, 5 and 10 wt% ND contents.

From the above results, we focused on pH of PSA/ND emulsion after ND aqueous dispersion was added into PSA emulsion. The ND was well-dispersed in aqueous solution in basic state, while it was aggregated in acidic state. While keeping constant pH of emulsion at 12, we prepared P(BA-AA)/ND PSA and their PSA properties were measured. Detailed properties were described in Table S4 in Supporting Information. Compared with P(BA-AA) PSA prepared at pH 12, the holding time and tack of P(BA-AA)/10wt%ND PSA were sustained. The peel strength of 1.3 N/cm for P(BA-AA)/0wt%ND increased to 4.1 N/cm for P(BA-AA)/10wt%ND PSA. The latter value of P(BA-AA)/10wt%ND PSA was almost equal to that of P(BA-GMA)/10wt%ND PSA. In addition, mechanical strength of P(BA-AA)/10wt%ND PSA prepared at pH 12 were also increased by ND loading, as shown in Figure S5 and Table S5 in Supporting Information. When we prepared PSA/ND emulsion under basic condition, ND would be dispersed even in P(BA-AA) PSA without any agglomeration and the well-dispersion led to the large effect of ND loading.

CONCLUSIONS

We demonstrated the adhesive properties of polyacrylate-based pressure-sensitive adhesives (PSAs) containing nanodiamond. The PSAs were prepared through soap-free emulsion polymerization, then nanodiamond was added into the PSA aqueous emulsion. P(BA-AA)/ND and P(BA-GMA)/ND composite PSAs were obtained. The ND loading led to increase of their PSA performance, in particular peel strength of P(BA-GMA)/ND, as well as their mechanical properties. Moreover, their thermal durability and thermal conductivity were also increased by ND loading. In the investigation of the morphology, ND in P(BA-GMA) PSA was well-dispersed and formed a network. This network led to a higher performance of P(BA-GMA)/ND PSA relative to P(BA-AA)/ND. It is revealed that the difference of performance between P(BA-GMA)/ND and P(BA-AA)/ND was attributed to the pH of PSA emulsion. High peel strength in P(BA-AA)/ND PSA system was also achieved by the control of acid-base condition.

ASSOCIATED CONTENT

Supporting Information.

This material is available free of charge via the Internet at.

AUTHOR INFORMATION

Corresponding Author

*(T.N.) E-mail: tnishino@kobe-u.ac.jp

Funding Sources

This work was partially supported by a Grant-in-Aid for Scientific Research (A) "High performance of environmentally friendly nanocomposites with post-carbon nanotube materials" (JP24246110).

Notes

The authors declare no competing financial interest.

ACKNOWLEDGEMENTS

We are grateful to Prof. Yoshinobu Nakamura and Prof. Shuji Fujii for the evaluation of PSA properties.

REFERENCES

1. Creton, C. *MRS Bull.* **2003**, *28*, 434.
2. Sun, S.; Li, M.; Liu, A. *Int. J. Adhes. Adhes.* **2013**, *41*, 98.
3. Creton, C.; Ciccotti, M. *Reports Prog. Phys.* **2016**, *79*, 46601.
4. Sherriff, M.; Knibbs, R. W.; Langley, P. G. *J. Appl. Polym. Sci.* **1973**, *17*, 3423.
5. Wang, T.; Colver, P. J.; Bon, S. A. F.; Keddie, J. L. *Soft Matter* **2009**, *5*, 3842.
6. Kim, J. K.; Kim, J. W.; Kim, M. I.; Song, M. S. *Macromol. Res.* **2006**, *14*, 517.
7. Gower, M. D.; Shanks, R. A. *J. Appl. Polym. Sci.* **2004**, *93*, 2909.
8. Viswanathan, G.; Chakrapani, N.; Yang, H.; Wei, B.; Chung, H.; Cho, K.; Ryu, C. Y.; Ajayan, P. M. *J. Am. Chem. Soc.* **2003**, *125*, 9258.
9. Shofner, M. L.; Khabashesku, V. N.; Barrera, E. V *Chem. Mater.* **2006**, *18*, 906.
10. Koziol, K.; Vilatela, J.; Moisala, A.; Motta, M.; Cunniff, P.; Sennett, M.; Windle, A. *Science (80-.).* **2007**, *318*, 1892 LP.
11. Stoneham, M. *Nat Mater* **2004**, *3*, 3.
12. Kim, S. J.; Choi, T.; Lee, B.; Lee, S.; Choi, K.; Park, J. B.; Yoo, J. M.; Choi, Y. S.; Ryu, J.; Kim, P.; Hone, J.; Hong, B. H. *Nano Lett.* **2015**, *15*, 3236.
13. Park, G. H.; Kim, K. T.; Ahn, Y. T.; Lee, H.; Jeong, H. M. *J. Ind. Eng. Chem.* **2014**, *20*, 4108.
14. Pang, B.; Ryu, C.-M.; Jin, X.; Kim, H.-I. *Appl. Surf. Sci.* **2013**, *285*, 727.
15. Hawełek, L.; Kołoczek, J.; Bródka, A.; Dore, J. C.; Honkimäki, V.; Burian, A. *Philos. Mag.* **2007**, *87*, 4973.
16. Hu, S.; Sun, J.; Du, X.; Tian, F.; Jiang, L. *Diam. Relat. Mater.* **2008**, *17*, 142.
17. Barnard, A. S.; Sternberg, M. *J. Mater. Chem.* **2007**, *17*, 4811.

18. Kaur, R.; Badea, I. *Int. J. Nanomedicine* **2013**, *8*, 203.

19. Osswald, S.; Yushin, G.; Mochalin, V.; Kucheyev, S. O.; Gogotsi, Y. *J. Am. Chem. Soc.* **2006**, *128*, 11635.

20. Lee, J.-Y.; Lim, D.-P.; Lim, D.-S. *Compos. Part B Eng.* **2007**, *38*, 810.

21. Bershtein, V.; Karabanova, L.; Sukhanova, T.; Yakushev, P.; Egorova, L.; Lutsyk, E.; Svyatyna, A.; Vylegzhanina, M. *Polymer.* **2008**, *49*, 836.

22. Korobov, M. V; Avramenko, N. V; Bogachev, A. G.; Rozhkova, N. N.; Ōsawa, E. *J. Phys. Chem. C* **2007**, *111*, 7330.

23. Okubo, M.; Nakamura, Y.; Matsumoto, T. *J. Polym. Sci. Polym. Chem. Ed.* **1980**, *18*, 2451.

24. Mishra, S.; Singh, J.; Choudhary, V. *J. Appl. Polym. Sci.* **2010**, *115*, 549.

25. Do, H.-S.; Park, J.-H.; Kim, H.-J. *J. Appl. Polym. Sci.* **2009**, *111*, 1172.

26. Ghosh, S.; Krishnamurti, N. *Eur. Polym. J.* **2000**, *36*, 2125.

27. Okubo, M.; Yamada, A.; Shibao, S.; Nakamae, K.; Matsumoto, T. *J. Appl. Polym. Sci.* **1981**, *26*, 1675.

28. Filippov, L. P. *Meas. Tech.* **1980**, *23*, 431.

29. Szybowicz, M.; Nowicka, A. B.; Sądej, M.; Andrzejewska, E.; Drozdowski, M. *J. Mol. Struct.* **2014**, *1070*, 131.

30. Merad, L.; Cochez, M.; Margueron, S.; Jauchem, F.; Ferriol, M.; Benyoucef, B.; Bourson, P. *Polym. Test.* **2009**, *28*, 42.

31. Yu, C.; Kim, Y. S.; Kim, D.; Grunlan, J. C. *Nano Lett.* **2008**, *8*, 4428.

32. Podsiadlo, P.; Kaushik, A. K.; Arruda, E. M.; Waas, A. M.; Shim, B. S.; Xu, J.; Nandivada, H.; Pumplin, B. G.; Lahann, J.; Ramamoorthy, A.; Kotov, N. A. *Science.* **2007**, *318*, 80 LP.

33. Morimune, S.; Kotera, M.; Nishino, T.; Goto, K.; Hata, K. *Macromolecules* **2011**, *44*, 4415.

34. TETSUMOTO, T.; GOTOH, Y. *J. Adhes. Soc. Japan* **2010**, *47*, 106.

35. Karimi Shamsabadi, M.; Moghbeli, M. R. *Int. J. Adhes. Adhes.* **2017**, *78*, 155.

36. Wang, T.; Lei, C.-H.; Dalton, A. B.; Creton, C.; Lin, Y.; Fernando, K. A. S.; Sun, Y.-P.; Manea, M.; Asua, J. M.; Keddie, J. L. *Adv. Mater.* **2006**, *18*, 2730.

TOC

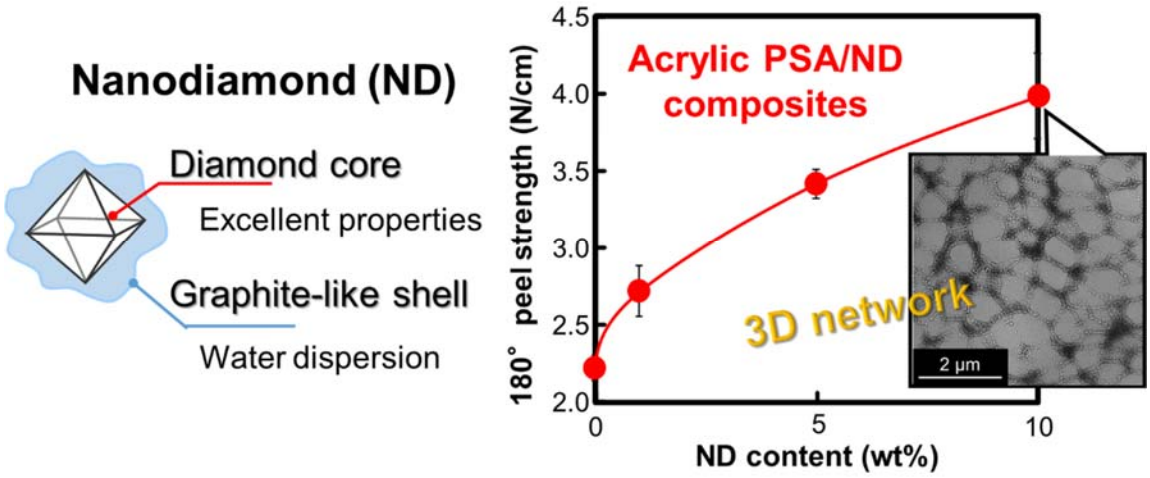
Nanodiamond (ND)
Diamond core
Excellent properties
Graphite-like shell
Water dispersion
Acrylic PSA/ND composites
3D network
2 μm
180° peel strength (N/cm)
ND content (wt%)
4.5
4.0
3.5
3.0
2.5
2.0
0
5
10